RESEARCH

Mebendazole inhibits tumor growth and prevents lung metastasis in models of advanced thyroid cancer

Tara Williamson[1,*], Thais Biude Mendes[2,*], Natalie Joe[1], Janete M Cerutti[2] and Gregory J Riggins[1]

[1]Departments of Neurosurgery and Oncology, Johns Hopkins University, Baltimore, Maryland, USA
[2]Genetic Bases of Thyroid Tumors Laboratory, Division of Genetics, Universidade Federal de São Paulo, São Paulo, Brazil

Correspondence should be addressed to J M Cerutti or G J Riggins: j.cerutti@unifesp.br or griggin1@jhmi.edu

*(T Williamson and T B Mendes contributed equally to this work)

Abstract

The most common thyroid malignancy is papillary thyroid cancer. While a majority respond to therapy and have a favorable prognosis, some papillary thyroid cancers persist. This subset may dedifferentiate to anaplastic thyroid cancer, an aggressive, highly invasive and rapidly fatal cancer. Thyroid cancer patients at risk for disease progression and metastasis need earlier, safer and more effective therapies. The purpose of this translational study was to determine if mebendazole could be repurposed to effectively treat thyroid cancer, in particular before metastasis. *In vitro*, mebendazole potently inhibited the growth of a panel of human papillary and anaplastic thyroid cancer cells. In papillary (B-CPAP) and anaplastic (8505c) cell lines, mebendazole increased the percentage of cells in G2/M cell cycle arrest and induced late stage apoptosis by activation of the caspase-3 pathway. In aggressive 8505c cells, mebendazole significantly repressed migratory and invasive potential in a wound healing and transwell invasion assay and inhibited expression of phosphorylated Akt and Stat3 and reduced Gli1. *In vivo*, mebendazole treatment resulted in significant orthotopic thyroid tumor regression (B-CPAP) and growth arrest (8505c), with treated tumors displaying reduced expression of the proliferation maker KI67 and less vascular epithelium as indicated by CD31+ immunohistochemistry. Most importantly, daily oral mebendazole prevented established thyroid tumors from metastasizing to the lung. Given the low toxicity and published anticancer mechanisms of mebendazole, this novel preclinical study of mebendazole in thyroid cancer has promising therapeutic implications for patients with treatment refractory papillary or anaplastic thyroid cancer.

Key Words

- mebendazole
- undifferentiated anaplastic thyroid carcinoma
- papillary thyroid carcinoma
- BRAF^{V600E} mutation
- lung metastasis

Endocrine-Related Cancer (2020) **27**, 123–136

Introduction

The major types of follicular cell–derived thyroid carcinomas are well-differentiated (papillary and follicular), poorly differentiated and undiferentiated (anaplastic) thyroid carcinoma – which vary considerably in their clinical outcome (Haddad *et al.* 2015). Papillary thyroid cancer (PTC) represents nearly 80% of cases, responds well to conventional treatment and in most cases carries an excellent prognosis (Melck *et al.* 2010). However, a rising number of PTC patients will suffer from recurrent or persistent disease (Bates *et al.* 2018).

https://erc.bioscientifica.com
https://doi.org/10.1530/ERC-19-0341

According to analysis of Surveillance, Epidemiology, and End Results (SEER) cancer registry data from 1980 to 2005, there has been a substantial increase in the incidence of advanced-stage papillary thyroid cancers (>5 cm in diameter), resulting in increased annual mortality rates in thyroid cancer in the United States (Lim *et al*. 2017).

PTC can progress to advanced poorly differentiated (PDTC) or anaplastic (ATC) subtypes without the proper treatment and these subtypes harbor a far worse prognosis (O'Neill & Shaha 2013). PDTC has an intermediate aggressiveness course between PTC and ATC. ATC is fast growing and one of the most lethal of all human cancers that represents ~2% of all thyroid cancers (Ragazzi *et al*. 2014). Given the rapid course of the disease and poor treatment outcomes, ATC is responsible for nearly half of all thyroid cancer deaths with a median survival of about 5 months and a 1-year survival rate of 20% (Keutgen *et al*. 2015). From its onset, ATC displays highly invasive behavior with a majority of patients exhibiting regional or distant metastases in the course of their disease, primarily to the lungs (Haddad *et al*. 2015). ATC is largely resistant to standard chemotherapy with most patients succumbing to uncontrolled local disease, metastatic disease or treatment-related toxicity (De Crevoisier *et al*. 2004, Nagaiah *et al*. 2011, Perri *et al*. 2011).

It has been suggested that molecular classification may explain the underlying characteristics observed in PTC, PDTC and ATC. The genomic landscape of PTC, recently reported by Cancer Genome Atlas Research Network (2014), showed that PTC is a tumor with one of the lowest tumor mutational burdens, and usually harbors only a single driver gene alteration. The author not only confirmed the significance of $BRAF^{V600E}$ or *RAS* mutations in the pathogenesis of PTC but also showed distinct signaling and transcriptome consequences in the two main molecular subtypes proposed. $BRAF^{V600E}$-like tumors showed a higher *MAPK* transcriptional output and lower expression of thyroid genes involved in idodine uptake and metabolism, as compared to that observed in *RAS*-like PTC (Cancer Genome Atlas Research Network 2014). These findings partially explain the more aggressive phenotype and increased patient mortality in $BRAF^{V600E}$-positive PTC (Xing 2013).

The genome and transcriptome analysis of PDTC and ATC confirmed that PDTC and ATC arise from differentiated PTC through the accumulation of key additional genetic activation mutations in TERT, EIF1AX, and PI3K pathway genes and inactivation of tumor suppressor genes *TP53*, *NF2* and *RB* (Landa *et al*. 2013, Song & Park 2019, Yoo *et al*. 2019). Although *BRAF* and *RAS* were the predominant drivers in PDTC and ATC, *TERT* promoter mutations and *TP53* were highly prevalence in advanced thyroid cancers harboring *BRAF* or *RAS* (Landa *et al*. 2013, Liu *et al*. 2013, Liu & Xing 2016). The coexisting $BRAF^{V600E}$ and *TERT* promoter mutations have a synergistic impact on the aggressiveness of thyroid carcinomas, including increased tumor recurrence and patient mortality (Landa *et al*. 2016, Liu *et al*. 2016).

The relationship between the $BRAF^{V600E}$ mutation, increased aggressiveness and poor responsiveness to standard therapies has been partly attributed to higher expression of vascular endothelial growth factor (VEGF) (Jo *et al*. 2006, Elisei *et al*. 2008). Thyroid tumors are highly vascularized and rely on VEGF/VEGFR2 signaling for adequate angiogenesis, extrathyroidal invasion, development of metastasis as well as activation of downstream effector pathways such as AKT, BRAF and STAT3 (Viglietto *et al*. 1995, Keefe *et al*. 2010, Perri *et al*. 2011). Therefore, several inhibitors of VEGF signaling pathways have been tested in radioactive iodine-refractory metastatic differentiated thyroid tumors and ATC (Cohen *et al*. 2008, Sherman *et al*. 2008). The aggressive pathology of ATC may be further explained by the presence of self-renewing cancer stem cells (Yun *et al*. 2014); a small population of cells in the tumor that can promote tumor chemo- and radioresistance and lead to high rates of recurrence and metastasis (Vicari *et al*. 2016). In addition, overactivation of sonic hedgehog (Shh) signaling promotes ATC motility and invasiveness (Williamson *et al*. 2016*a*).

Mebendazole (MBZ) is a FDA-approved benzimidazole with an excellent safety profile that has been widely used to treat parasitic infections. The anthelmintic action of MBZ is primarily attributed to its ability to bind tubulin and inhibit microtubule polymerization, an effect that has also correlated with anti-proliferative activity against cancer cells, *in vitro* (Mukhopadhyay *et al*. 2002, Bai *et al*. 2011). MBZ has been repositioned for use in oncology (Pantziarka *et al*. 2014) because it exhibits preclinical anticancer activity, not only through its known molecular target of tubulin, but also through its off-target ability to bind and inhibit signaling of select tyrosine kinases: VEGFR2, TNIK and BRAF (Nygren *et al*. 2013, Bai *et al*. 2015, Tan *et al*. 2016, Simbulan-Rosenthal *et al*. 2017). Other reported tumor suppressive mechanisms of MBZ include induction of cell cycle arrest, inhibition of tumor neovascularization, inhibition of the Shh pathway and activation of apoptosis through BCL-2 and caspase-3-dependent mechanisms (Sasaki *et al*. 2002, Doudican *et al*.

https://erc.bioscientifica.com
https://doi.org/10.1530/ERC-19-0341

2008, 2013, Bai *et al*. 2015, Larsen *et al*. 2015, Pinto *et al*. 2015).

MBZ appears to work by targeting multiple oncogenic pathways in cancer cells without the risk of serious side effects (Mudduluru *et al*. 2016). Evidence supports the use of MBZ for treatment of brain and colon cancers, both in a therapeutic and preventative context, respectively (Bai *et al*. 2011, 2015, Williamson *et al*. 2016*b*). Clinical trials using MBZ in glioblastoma, recurrent pediatric brain tumors and colon cancer are currently underway (NCT01729260, NCT02644291, NCT03628079). Additionally, clinical case studies of MBZ usage resulted in disease stabilization and tumor regression in refractory metastatic colorectal cancer and metastatic adrenocortical carcinoma (Dobrosotskaya *et al*. 2011, Nygren & Larsson 2014). We investigated the utility of MBZ as a therapy to treat advanced or refractory thyroid cancers.

In this translational study, we determined MBZ drug sensitivity and effect on *in vitro* cell proliferation in a panel of human PTC (B-CPAP and TPC1) and ATC (8505c and KTC-2) cell lines. B-CPAP and 8505c cell lines were subjected to further investigation to analyze the effect of MBZ on cell cyle arrest and apoptosis. Aggressive 8505c cells were treated with MBZ and the resulting effect on metastatic potential and select pathways that drive thyroid tumor progression were determined. We then investigated the *in vivo* effects of daily MBZ treatment on thyroid tumor growth and pulmonary metastasis in orthotopic models of B-CPAP as well as 8505c and analyzed treated tumors for markers of proliferation and angiogenesis.

Materials and methods

Cell culture

8505c (ACC 219) and B-CPAP (ACC 273) cell lines were purchased from DSMZ (Germany). TPC1 cell line was donated by Dr Joao R Maciel (Federal University São Paulo, São Paulo, Brazil). KTC-2 cell line was donated by Prof. Junichi Kurebayashi (Kawasaki Medical School, Japan) (Kurebayashi *et al*. 2003). Short tandem repeat (STR) sequencing of cell lines was performed to check for cross contamination (Saiselet *et al*. 2012, Schweppe 2012). B-CPAP, TPC1 and 8505c cells were grown in RPMI-1640 medium supplemented plus 10% FBS. KTC-2 cells were grown in RPMI-1640 medium supplemented plus 5% FBS. Cells were maintained at 37°C in a 5% CO_2 humidified atmosphere.

Mebendazole IC_{50}, proliferation

To obtain the half-maximal inhibitory concentrations (IC_{50}) values, B-CPAP, TPC1, 8505c and KTC-2 cells were seeded in 96-well plates (2500/well), cultured for 24 h, then exposed to a range of MBZ concentrations (1 nM - 100 µM) and 1% DMSO (vehicle control). The absorbance of the cells was measured after 48 h and the MBZ IC_{50} was calculated using GraphPad Prism 5 software. To measure proliferation, cells were seeded (10^3) in 96-well plates cultured for 24 h before being exposed to MBZ (0.5 µM) and DMSO (control). The proliferation rate was measured by estimating cell viability every 24 h up to 96 h. The number of live cells present in each assay listed above was estimated by using the Cell Counting Kit-8 (CCK8) Assay (Dojindo Laboratories) and measured at an absorbance of 450 nm on a PerkinElmer VICTOR3 plate reader, according to the manufacture's instructions, as previously described (Bai *et al*. 2011).

Cell cycle analysis

Cell cycle analysis was performed using propidium iodide staining. B-CPAP and 8505c cells were cultured and treated with 0.5 µM, 1 µM MBZ or vehicle control for 24 h, washed with PBS and fixed in 70% ethanol overnight at 4°C. Cells were pelleted, washed twice with PBS, and stained with 5 µg/mL RNase and 50 µg/mL of propidium iodide (Abcam) in the dark at 37°C for 30 min. The distribution of cells in sub-G1, G1, S and G2/M phases and cells in the 8 N population were determined by flow cytometry on a LSRFortessa cell analyzer (BD Biosciences) and data analysis was performed using the Watson pragmatic model in FlowJo software v10.5.3.

Apoptosis assay

Measurements of viable, early apoptotic and late apoptotic cells were performed on B-CPAP and 8505c cells exposed to 0.5 µM, 1 µM MBZ or vehicle control for 48 h in culture. Cells were detached with Accutase, washed twice with PBS and resuspended in binding buffer and double stained with 5 µL of APC-conjugated Annexin V and 5 µL 7-amino-actinomycin D (7-AAD), per manufacturer's instructions (BD Pharmigen). Cells were collected by flow cytometry on a BD LSRFortessa cell analyzer and the percentage of cells undergoing apoptosis was determined using FlowJo single-cell analysis software v10.5.3.

https://erc.bioscientifica.com
https://doi.org/10.1530/ERC-19-0341

Western blotting

Cell homogenates prepared from B-CPAP and 8505c cell lines were incubated on ice in radio-immunoprecipitation (RIPA) buffer supplemented with protease and phosphatase inhibitor cocktails and centrifuged at 10,000 ***g*** for 10 min. Protein concentration was quantified using the BCA protein assay kit (Pierce Biotechnology). Thirty micrograms of reduced protein was loaded into a 4–12% NuPage Bis-Tris gel (Invitrogen) and subsequently transferred to a PVDF membrane (BioRad) and blocked for 1 h in TBS with 0.1% Tween/5% nonfat dry milk prior to probing with the following primary antibodies: XIAP, caspase 3, cleaved-caspase 3 (CI-Caspase 3), PARP, cleaved PARP (CI-PARP), total ERK, p-ERK (Thr202/204), total Akt, p-Akt (Ser473), total STAT3, p-STAT3 (Y705), Gli1 and GAPDH (Cell Signaling Technologies). Primary antibodies were incubated overnight at 4°C in blocking buffer then washed and incubated with anti-rabbit horseradish peroxidase-conjugated secondary antibodies for 1 h prior to detection. Signals were visualized using enhanced chemiluminescent reagents according to manufactures instructions (SuperSignal, Thermo Scientific).

Wound healing

8505c cells were cultured in 100 mm culture dishes until they reached near confluence. Multiple linear scratches of equal width were introduced through the confluent cells using a 100 µL pipette. Cells were washed to remove debris and then exposed to 0.5 µM MBZ or vehicle control. A photomicrograph was taken at five locations in each dish at 0 h and 24 h to compare differences in cell migration. The distance of cell migration was measured for each condition and percent relative wound closure rate was estimated to determine the effect of MBZ on cell mobility.

Transwell invasion assay

Transwell invasion assays were performed using a Biocoat matrigel matrix (BD Biosciences) 8-µm pore size, PET membrane in a 24-well plate, according to the manufacturer's instructions (Corning). The lower chambers of the transwell plates were filled with 750 µL RPMI 1640 medium containing 10% FBS. Following detachment of 8505c cells from tissue culture plates, cells were resuspended in RPMI 1640 medium containing 1% FBS and then loaded onto the upper side of the chamber (2.5×10^4 cells/well in 500 µL media). Transwells were placed in incubators at 37°C for 24 h. The cells on the upper surface of filters were removed using cotton swabs and those on the lower surface were stained with 0.1% crystal violet and counted. Cells that invaded were counted in five random fields of each filter under a microscope.

Luciferase expression

A lentiviral construct with firefly luciferase cDNA was transfected into B-CPAP and 8505c cell lines, with 8 mg/mL polybrene (Sigma Aldrich) in RPMI 1640 media. Cells were maintained at 37°C in a 5% CO_2 humidified atmosphere. After 24 h, the cells were harvested and the presence of luminescence was confirmed on a VICTOR3 plate reader. Luciferase-positive cells were further expanded for use in the orthopic thyroid model.

Orthotopic study

All animal experiments were performed according to approved Johns Hopkins Animal Care and Use protocols. For orthopic thyroid implantation, 10-week-old female athymic nude mice were anesthetized using an intraperitoneal injection of ketamine hydrochloride (100 mg/mL) and xylazine (100 mg/mL) diluted in a 10:1 ratio with 0.9% saline. Thyroid cell implantation was performed as previously described (Nucera *et al.* 2009). Briefy, the neck was washed with betadine and a 1 mm vertical incision was made through the skin and s.c. tissues. The strap muscles were bluntly dissected away to expose the trachea and thyroid glands. One million luciferase-expressing cells were resuspended in 10 µL serum-free media implanted into the right thyroid gland using a Hamilton Syringe (B-CPAP, $n=12$ mice) and (8505c, $n=12$ mice). Following the implantation, the neck muscles were repositioned and the incision was closed using three nylon sutures. Five days after implantation, thyroid tumor establishment was confirmed by luminescence and the mice were randomized into Control and MBZ, $n=6$ mice per group, with equivalent baseline radiance values. Both control and treatment groups were given standard mouse meal with added water and seasame oil (at a 4:1 ratio) necessary for mixing. Seasame oil was supplemented to aid in the absorption of MBZ (Bai *et al.* 2011). The control mice received untreated feed and the MBZ mice received feed containing 50 mg/kg of mebendazole. Daily MBZ treatment continued starting on Day 5 post-implantation and continued for the duration of the study. Fresh food was prepared 3× per week and daily consumption was calculated to confirm drug dose.

https://erc.bioscientifica.com
https://doi.org/10.1530/ERC-19-0341

In vivo and *ex vivo* luciferase activity

Intrathyroidal luciferase activity was measured weekly during the course of the study by injecting the mice with 150 µL (2 µg/mouse) of D-luciferin potassium salt (Gold Bio) in PBS. Mice were then briefly anesthetized with Flurido (Isoflurane, USP) and bioluminescence values were acquired using a Xenogen (IVIS 200, equipped with Living Image Software) within 10 min of luciferin injection, as described previously (Bai *et al*. 2011). All tumor bioluminescence values were expressed as radiance (photons/second) and graphed to monitor tumor growth *in vivo*. At the conclusion of the study, the last *in vivo* measurement was taken and the mice were killed and the thyroid tumor and lungs were quickly harvested. The lungs were immediately placed back in the Xenogen IVIS and exposed for 5 min to visualize *ex vivo* luminescence for detection of metastasis.

Histology and immunohistochemistry

Thyroid and lung tissues from orthotopic study were placed in 10% formalin at the time of necropsy for subsequent histological analysis. Hematoxylin and eosin (H&E) slides were prepared from experimental tissue and scanned at 20× using a Aperio AT2 slide scanner. Thyroid tumor size was estimated by measuring length and width of tumors from 20× scanned images of H&E sections using the ImageScope software and tumor size was expressed in square millimeters ($L \times W = mm^2$). For immunohistochemistry, paraffin-embedded thyroid tumor slides were deparaffinized with xylene and hydrated through a graded alcohol series. Endogenous peroxidase activity was blocked with 3% hydrogen peroxide (Fisher Scientific) for 10 min. Antigen retrieval was performed using Antigen Retrieval Citra Solution pH 6 (BioGenex) in heat cooker for 30 min, followed by avidin/biotin block (Life Technologies) with 10% goat serum + 1% BSA in PBS and incubated for 30 min. Primary antibody Ki67 (1:500, Abcam) and CD31 (1:50, Thermo Fisher) were incubated overnight. Immunostaining was performed using Super Sensitive™ IHC Detection Systems (BioGenex). Slides were counterstained with hematoxylin and analyzed using a light microscope and scanned at 20× using an Aperio AT2 slide scanner. Ki67 staining intensity was measured using ImageJ and the values for three images from $n = 5$ animals per group were averaged. To analyze microvessel density (MVD), tumor sections were viewed under 20× magnification to identify microvessel 'hotspots' of CD31-positive endothelial cells and the average MVD was calculated from ten fields from each treatment group.

Statistical analysis

The results were subjected to Shapiro–Wilk Normality Test. Student's *t*-test was used for normally distributed data and Mann–Whitney for data not normally distributed. Values were considered significantly different with a $P < 0.05$. We used GraphPad Prism 5 (GraphPad Software) and SigmaPlot 12.0 (Systat Software Inc) for statistics.

Results

Mebendazole reduced proliferation and viability of human thyroid cancer cell lines

MBZ IC_{50} values for human papillary thyroid cell lines B-CPAP and TPC1 were 57 nM and 327 nM, respectively (Fig. 1A and B). For the 8505c and KTC-2 anaplastic thyroid cancer cell lines, the MBZ IC_{50} values were 472 nM and 146 nM, respectively (Fig. 1C and D). Cell proliferation measured at multiple time points using CCK8 assay revealed that MBZ (0.5 µM) caused significant and sustained cell growth inhibition of 89 and 69% in B-CPAP and TPC1 papillary cell lines, respectively (Fig. 1E and F) and an inhibition of 89 and 72% in 8505c and KTC-2 anaplastic cell lines, respectively (Fig. 1G and H), compared to controls (Fig. 1). These results are consistent with previously published data showing that MBZ can elicit anti-proliferative effects *in vitro* in a variety of cancer cell lines at concentrations ranging from 0.1 µM to 0.8 µM, regardless of mutation (Mukhopadhyay *et al*. 2002, Williamson *et al*. 2016*b*). The cell lines and their respective MBZ IC_{50} values and driver mutations are summarized in Fig. 1I.

Mebendazole induced G2/M cell cycle arrest and caspase 3-dependent apoptosis in thyroid cancer cells

We next investigated whether MBZ induces cell cycle arrest in B-CPAP and 8505c cell lines using propidium iodide staining. At 0.5 µM, MBZ increased the percentage of cells in G2/M phase mitotic arrest by 8.9% in B-CPAP ($P = 0.0036$) and 1% in 8505c (ns) versus vehicle control-treated cells. At 1 µM, MBZ significantly increased the percentage of cells in G2/M phase mitotic arrest by 44.9% in B-CPAP ($P < 0.0001$) and 9.9% in 8505c ($P = 0.0204$) compared to vehicle control cells (Fig. 2A and B). MBZ was able to disrupt cell division in both thyroid cancer cell lines, with B-CPAP cells displaying enhanced sensitivity. The number of 8505c cells in the 8 N population increased in a dose-dependent manner when treated with

https://erc.bioscientifica.com
https://doi.org/10.1530/ERC-19-0341

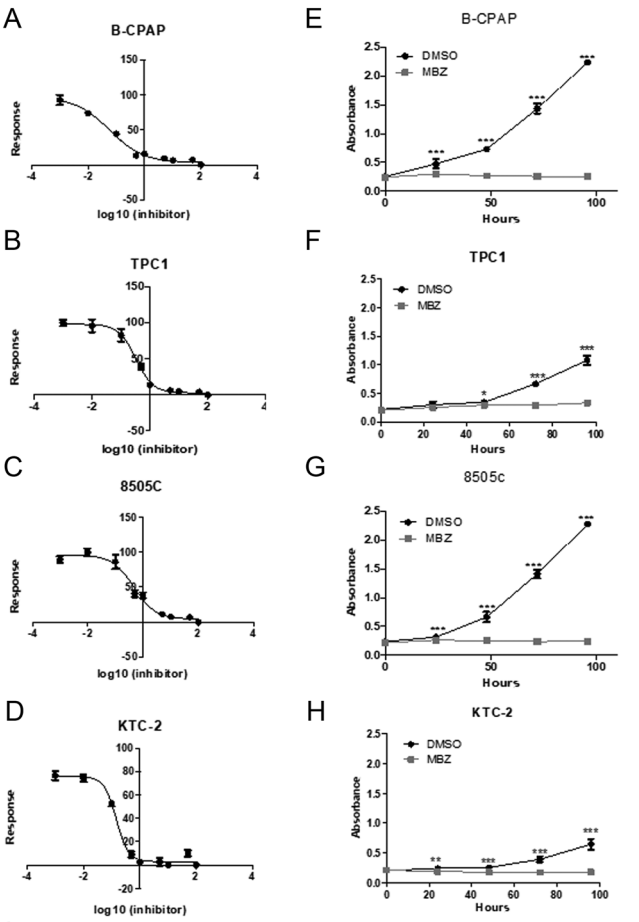

I

Cell Line	Subtype	Mutations	MBZ IC_{50}
B-CPAP	PTC	$BRAF^{V600E}$, $Tp53^{D259Y}$, TERT c. C228T	57 nM
TCP1	PTC	RET/PTC1, Tp53 wild type	327 nM
8505c	ATC	$BRAF^{V600E}$, $Tp53^{R248G}$, $NF2^{E129T}$, TERT c. C250T	472 nM
KTC-2	ATC	$BRAF^{V600E}$, $KMT2D^{E490T}$, TERT c.228T	146 nM

Figure 1
Mebendazole reduced cell proliferation in papillary and anaplastic thyroid cancer cell lines. The half-maximal inhibitory concentration (IC_{50}) of MBZ in (A) B-CPAP, (B) TPC1, (C) 8505c and (D) KTC-2. Cell proliferation was measured at multiple time points using CCK8 assay up until 96 h after exposure to 0.5 µM MBZ in (E) B-CPAP, (F) TPC1, (G) 8505c and (H) KTC-2 cells. Summary of cell line comparison (I) Data respresent mean ± S.D. *P* values *<0.05, **<0.01, ***<0.0001.

MBZ which is likely due to mitotic slippage caused by microtubule inhibition.

To compare rates of apoptosis, B-CPAP and 8505c cells were treated with MBZ for 48 h, stained with Annexin V/7-AAD and analyzed by flow cytometry. Figure 3A shows representative dot plots displaying the percentage of cells undergoing early and late stage apoptosis for vehicle control, 0.5 µM MBZ and 1 µM MBZ-treated cells. Compared to controls, 0.5 µM MBZ resulted in 17 and 0.8% increases in the percentage late apoptotic cells in B-CPAP (P=0.0009) and 8505c (ns), respectively. Compared to controls, 1 µM MBZ resulted in 40.8 and 6.4% increases in the percentage late apoptotic cells in B-CPAP (P=0.0003) and 8505c (P=0.0239), respectively (Fig. 3B). As MBZ has been previously shown to selectively induce tumor cell apoptosis via caspase-dependent mechanisms (Sasaki *et al.* 2002, Doudican *et al.* 2013, Skibinski *et al.* 2018), treated cells were probed for markers of apoptosis. Expression of XIAP, a negative regulator of caspase activation, was reduced in B-CPAP cells following MBZ treatment, resulting in significant upregulation of cleaved (activated) caspase 3 and cleaved PARP, even at low (0.25 µM) MBZ concentrations. XIAP expression remained unchanged in MBZ treated 8505c cells and changes in expression of cleaved-caspase and cleaved-PARP followed a more dose-dependent pattern (Fig. 3C). Our *in vitro* data indicate that B-CPAP is sensitive to MBZ-induced apoptosis, while 8505c cells exhibited greater resistance to apoptosis at lower MBZ concentrations. However, MBZ did induce apoptosis more effectively in 8505c cells than the commonly used BRAF inhibitor, vemurafenib (PLX4032), as indicated by increased expression of cleaved-PARP following 24 h and 6 days of exposure at equivalent drug concentrations (0.5 µM and 1 µM) (Fig. 3D).

Mebendazole suppresses metastatic potential of 8505c and reduces PI3K/Akt and STAT3 signaling

To investigate whether MBZ could inhibit invasive potential of thyroid cancer cell lines, we utilized highly metastatic 8505c cells in *in vitro* assays of migration and invasion. 8505c cells were exposed to MBZ (0.5 µM) for 24 h and the relative wound closure rate was compared to that of vehicle control treated cells. MBZ significantly reduced 8505c cell migration potential compared to control (P<0.0001) (Fig. 4A and C). Furthermore, 0.5 µM and 1 µM MBZ significantly inhibited the number of cells that migrated through a Matrigel membrane over 24 h compared to control cells (P<0.0001) (Fig. 4B and D). MBZ-treated 8505c cells were probed for effectors of the MAPK, PI3K–AKT, STAT3 and Hedgehog signaling pathways. MBZ reduced expression of p-Akt (Ser473), p-Stat3 (Y705) and Gli1, but did not alter expression of p-ERK (Thr202/204) (Fig. 4E).

Mebendazole inhibits tumor growth and blocks lung metastases in orthotopic models of papillary and anaplastic thyroid cancer

Orthotopic models of thyroid cancer are commonly used to test systemic therapies as they faithfully recapitulate

https://erc.bioscientifica.com
https://doi.org/10.1530/ERC-19-0341

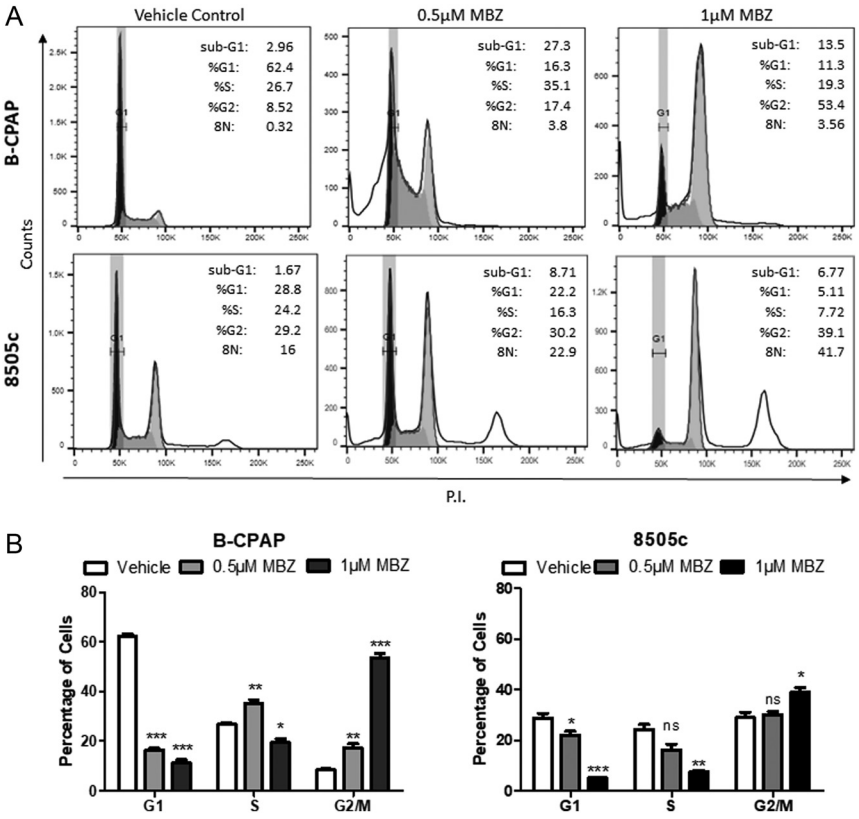

Figure 2
Mebendazole induces G2/M cell cycle arrest in human papillary and anaplastic thyroid cancer cell lines. (A) Representative histogram plots of cell cycle alterations in B-CPAP and 8505c cells treated with 0.5 μM and 1 μM MBZ or DMSO vehicle control for 24 h. (B) The percentage of cells in each phase of cell cycle at 0.5 μM and 1 μM MBZ were graphed. Data represent mean ± S.D. *P* values *<0.05, **<0.01, ***<0.0001.

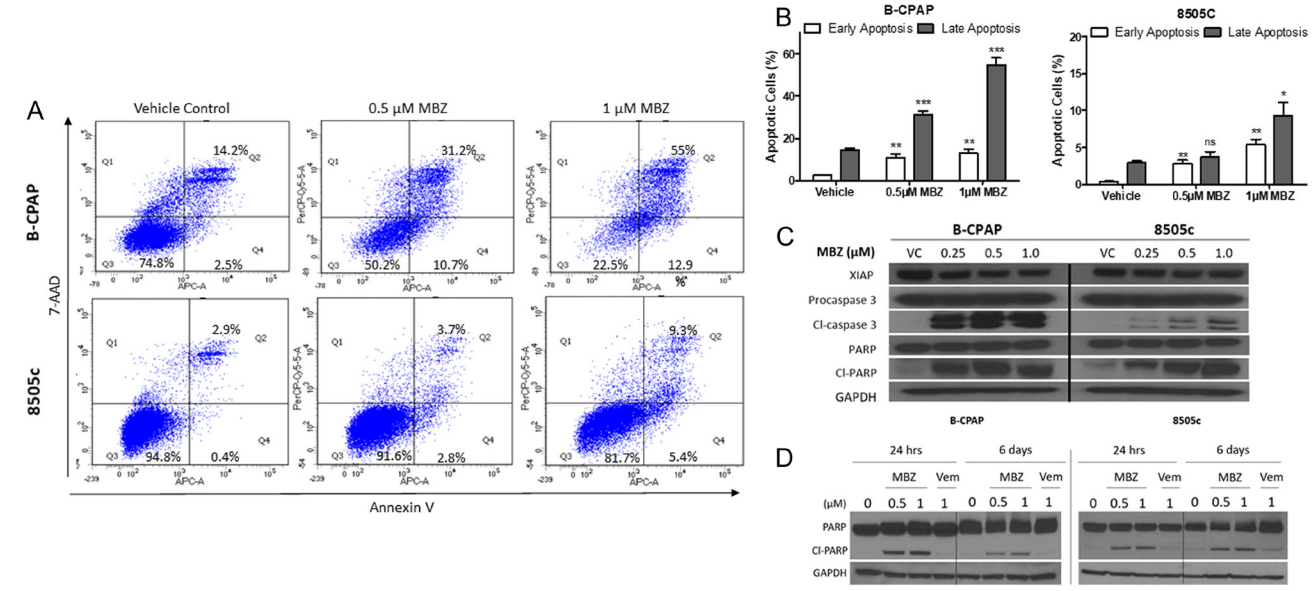

Figure 3
MBZ induces caspase 3-dependent apoptosis in aggressive thyroid cancer cells. B-CPAP and 8505c cells were treated with 0.5 μM and 1 μM MBZ or DMSO vehicle control for 48 h and apoptosis was analyzed by flow cytometry using APC Annexin V/7-AAD. (A) Representative dot plot of apoptosis assay by flow cytometry. (B) The percentage of cells undergoing early and late apoptosis at each MBZ concentration were graphed. (C) Expression of proteins involved in MBZ-induced apoptosis were analyzed by Western blot, with GAPDH as the loading control. (D) Expression of PARP/cleaved-PARP was compared in 8505c cells treated with Mebendazole (MBZ) or Vemurafenib (VEM) for 24 h and 6 days to compare activation of apoptosis. Data represent mean ± S.D. *P* values *<0.05, **<0.01, ***<0.0001. A full colour version of this figure is available at https://doi.org/10.1530/ERC-19-0341.

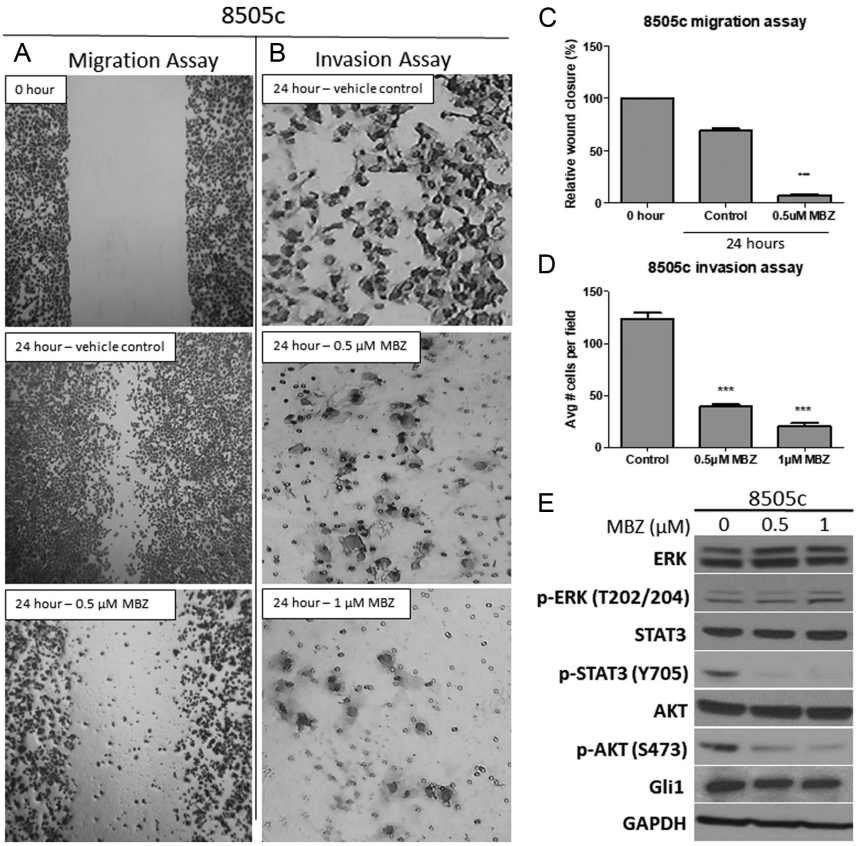

Figure 4
Mebendazole suppresses metastatic potential of anaplastic 8505c cells and inhibits p-Akt, p-STAT3 and Gli1 expression. Wound healing and transwell assay were used to test the ability of MBZ to inhibit migration and invasion of 8505c cells after 24 h of treatment. (A) Representative photomicrograph of wound healing. (B) Representative photomicrograph of transwell assay. (C) Analysis of relative wound closure of the cells after treatment with MBZ or Control. (D) Analysis of average cells per field in the each group. (E) Representative blot of ERK (total and p-Thr202/204), AKT (total and p-Ser473), STAT3 (total and p-Y705) and Gli1 determined by Western blot with GAPDH as the loading control. Data represent mean ± S.D. ***$P < 0.0001$.

the clinical presentation of rapid tumor growth, tracheal and esophageal compression, laryngeal and tracheal invasion, cachexia, and high incidence of local and distant metastasis seen in the human disease (Kim *et al.* 2005, Antonello & Nucera 2014). Orthotopic xenografts were established in athymic nude mice using luciferase-expressing B-CPAP and 8505c cells. Bioluminescent images from control and MBZ-treated mice were acquired at weekly intervals over the course of the study to monitor tumor growth (Figs 5A and 6A). Following a 5-day establishment period, mice were randomized and given either control or daily 50 mg/kg MBZ in the feed for 42 days (B-CPAP) and 28 days (8505c) and the experiment was terminated when control mice began exhibiting signs of cachexia.

In the B-CPAP papillary thyroid cancer model, the tumors of the untreated mice displayed a significant increase in radiance 20 days post implantation and the tumors continued to grow steadily, with a sharp rise in tumor radiance between days 40–49 post implantation (Fig. 5B). In contrast, the imaging of MBZ-treated B-CPAP mice showed a marked reduction in radiance after 14 days of treatment and the radiance was completely undetectable in four mice and nearly undectectable in two mice at the end of the study (Fig. 5A). Overall, MBZ treatment of B-CPAP orthotopic tumors resulted in a 99% ($P=0.0072$) radiance decrease compared to control (Fig. 5B). Thyroid tumors were palpable in 83% (5/6) untreated B-CPAP mice and H&E sections revealed massive primary tumors (median size 45.5 mm^2) that were invading locally into the surrounding tissue (Fig. 5C). In contrast, MBZ-treated B-CPAP mice did not have palpable tumors and H&E sections revealed small, microscopic tumors embedded in the thyroid (median size 0.041 mm^2) or no tumor (Fig. 5C). The left thyroid and surrounding tissues were unaffected in MBZ-treated mice. *Ex vivo* analysis of lung tissue revealed bioluminescent metastatic lesions in 83% (5/6) of the mice in the B-CPAP control group, whereas there was no detectable luminescence in the lungs of MBZ-treated mice (Fig. 5D). H&E-stained lung tissue sections were used to verify the presence of multiple micrometastic lesions in the control group and unaffected lung tissue in MBZ-treated mice (Fig. 5E).

In the 8505c, orthotopic model of anaplastic thyroid cancer, weekly *in vivo* bioluminescent images obtained over the course of the study (Fig. 6A) showed the rapid course of the disease as thyroid tumors in untreated mice grew in a predictable, aggressive manner (Antonello &

https://erc.bioscientifica.com
https://doi.org/10.1530/ERC-19-0341

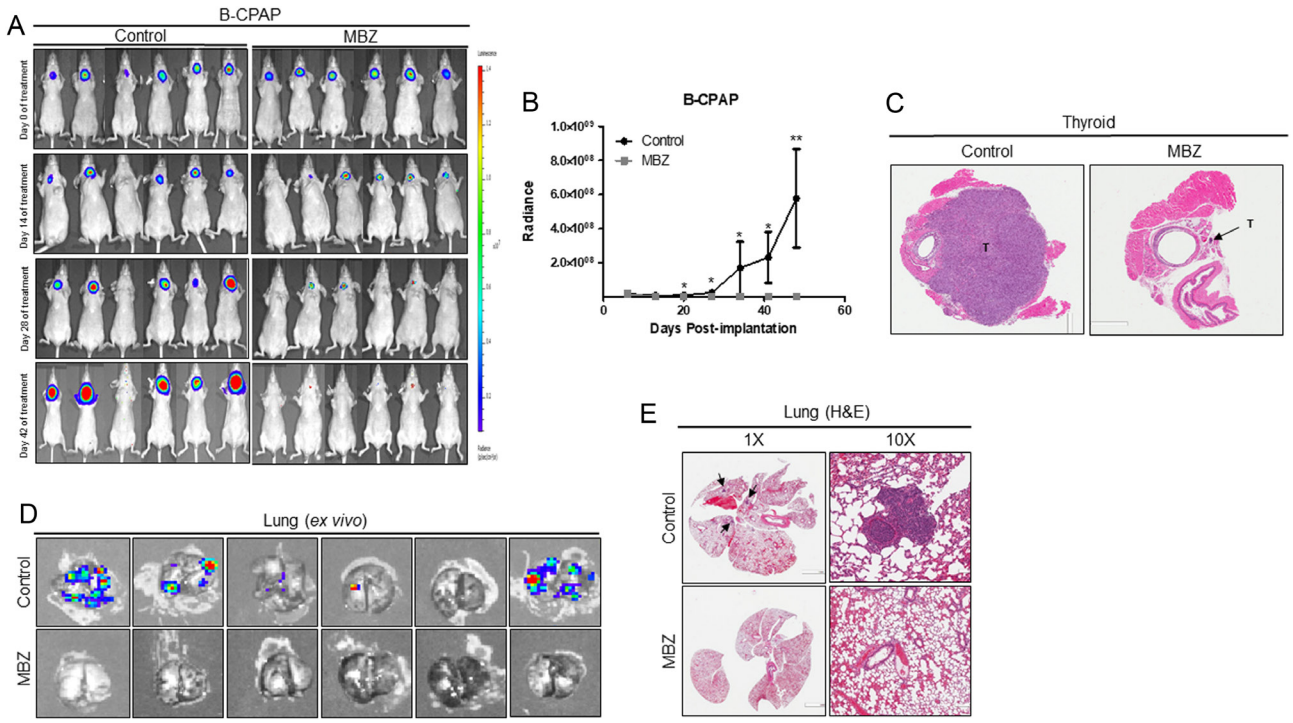

Figure 5

Mebendazole inhibits primary tumor growth and metastasis to lungs in orthotopic model of papillary thyroid cancer. (A) One million luciferase expressing B-CPAP cells were implanted into the right thyroid of nude mice and *in vivo* bioluminescence was obtained weekly to monitor tumor growth between control and 50 mg/kg MBZ-treated mice. (B) Thyroid intratumoral luminescence was graphed during 42 days of treatment. (C) At the end of the study, thyroid and surrounding tissue were extracted for histological analysis revealing large tumors in the Control group (T) and small microtumors in MBZ group (indicated by arrow). (D) The lungs were removed for *ex vivo* bioluminescent imaging of metastasis and (E) histological evaluation of pulmonary metastatic lesions. Data represents mean ± S.D. *P* values *<0.05, **<0.01.

Nucera 2014, Morrison *et al*. 2015). Radiance values from 8505c control mice began to significantly increase 20 days post implantation, followed by a sharp growth period between day 28 and 35 post implantation (Fig. 6B). It was during this time that the control mice presented with evidence of the mass effect of the tumor on the trachea and invasion to the lungs. All 100% (6/6) of mice in the control group had large, palpable tumors on day 35. In the MBZ group, the treatment inhibited tumor growth and stabilized radiance values, resulting in a 96% (P=0.0140) reduction in final intratumoral luminescence at 35 days post implantation when compared with control mice (Fig. 6A and B). Analysis of H&E sections confirmed that the control 8505c mice had large, infiltrating primary thyroid tumors (median size 29.9 mm^2) that were locally invading the trachea and left thyroid (Fig. 6C). MBZ-treated 8505c mice had small tumors (median size 1.71 mm^2) that were confined to the right thyroid only with no indication of local invasion (Fig. 6C). During the *ex vivo* lung analysis, the presence of pulmonary mestastases was vividly detected via luminescence in 100% (6/6) of mice in the control group, whereas in the MBZ-treated group there was no evidence of metastasis (Fig. 6D). H&E staining of lung tissue allowed visualization of widespread metastasis in the control mice, which was not observed in the MBZ-treated mice (Fig. 6E). The results of our orthotopic mouse studies show that MBZ suppresses thyroid tumor growth and blocks lung metastasis in two aggressive, BRAF, TP53, TERT-mutant models.

Mebendazole decreases markers of tumor proliferation and vascularization in anaplastic thyroid carcinoma

The tumors derived from the 8505c thyroid studies were further analyzed for markers of proliferation (Ki67) and microvessel density (CD31) (Fig. 7A). Immunohistochemical analysis of Ki67 was used to visualize MBZ effects on cell proliferation *in vivo*, to correlate with induction of mitotic arrest, *in vitro* (Mukhopadhyay *et al*. 2002, Sasaki *et al*. 2002). MBZ decreased Ki67 staining intensity in 8505c orthotopic tumors by 61% (P=0.0007) compared to untreated controls (Fig. 7B). It has been previously shown that MBZ acts as a kinase inhibitor

https://erc.bioscientifica.com
https://doi.org/10.1530/ERC-19-0341

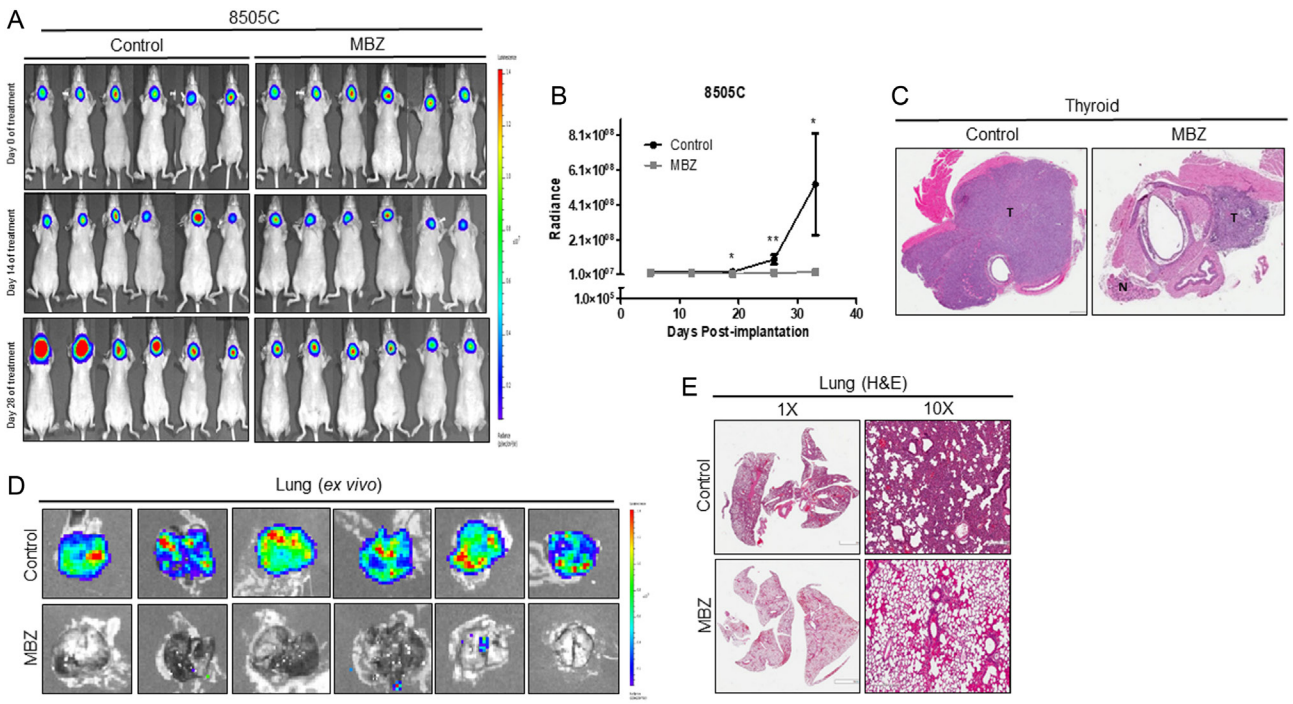

Figure 6

Mebendazole inhibits primary tumor growth and metastasis to lung in orthotopic model of anaplastic thyroid cancer. (A) One million luciferase expressing 8505c cells were implanted into the right thyroid of nude mice and *in vivo* bioluminescence was obtained weekly to monitor tumor growth between control and 50 mg/kg MBZ-treated mice. (B) Thyroid intratumoral luminescence was graphed during 28 days of treatment. (C) At the end of the study, the thyroid and surrounding tissue were extracted for histological analysis revealing large, infiltrating tumors in the Control group (T) compared to smaller tumors and normal left thyroid (N) in the MBZ group. (D) The lungs were removed for *ex vivo* bioluminescent imaging of metastasis and (E) histological evaluation of pulmonary metastatic lesions. Data represent mean ± S.D. *P* values *<0.05, **<0.01.

against VEGFR2 and reduces tumor angiogenesis (Bai *et al.* 2015, Williamson *et al.* 2016*b*). To measure effects on the tumor vasculature, we calculated microvessel density in tumor sections stained with the anti-CD31 (PECAM1) antibody. MBZ significantly decreased CD31-positive endothelial staining in 8505c orthotopic thyroid tumors 47% (P=0.0202) (Fig. 7C). It should be noted that control B-CPAP thyroid tumors also showed intense Ki67 and CD31 positivity (data not shown) but lack of sufficient tumors in MBZ treated B-CPAP mice did not allow for an evaluation of treatment effect. Therefore, only 8505c tumors were subjected to comparative analysis.

Discussion

Our preclinical findings indicate that a non-toxic oral benzimidazole, mebendazole, can suppress primary thyroid tumor growth and prevent pulmonary metastasis. This has important clinical implications for the 20–30% of PTC patients (12,000–18,000 patients in the United States) who are at risk of developing persistent or progressive disease, which could dedifferentiate into a more aggressive undifferentiated phenotype with lower survival rates (Melck *et al.* 2010, Czarniecka *et al.* 2016, Bates *et al.* 2018). There are limited FDA-approved drugs for patients with advanced or recurrent thyroid cancer and the evolving treatment regimens have yet to have a significant impact (Keutgen *et al.* 2015, Saini *et al.* 2018). In recent years, there has been extensive clinical testing of targeted kinase inhibitors as second-line therapies (Sherman 2011, Guerra *et al.* 2013, Hsu *et al.* 2014, Alonso-Gordoa *et al.* 2015), but many of these therapies fail due to drug resistance or unacceptable drug toxicity (Viola *et al.* 2016).

In this study, we demonstrated that oral mebendazole polymorph C can effectively inhibit the growth and viability of thyroid cancer cells at nanomolar concentrations, *in vitro*. The MBZ IC_{50} values for papillary thyroid cancer cell lines, B-CPAP and TPC1, were 57 nM and 327 nM, respectively, and for anaplastic thyroid cancer cell lines, 8505c and KTC-2, were 472 nM and 146 nM, respectively. This data indicates a difference in drug sensitivity between the all cell lines, although

https://erc.bioscientifica.com
https://doi.org/10.1530/ERC-19-0341

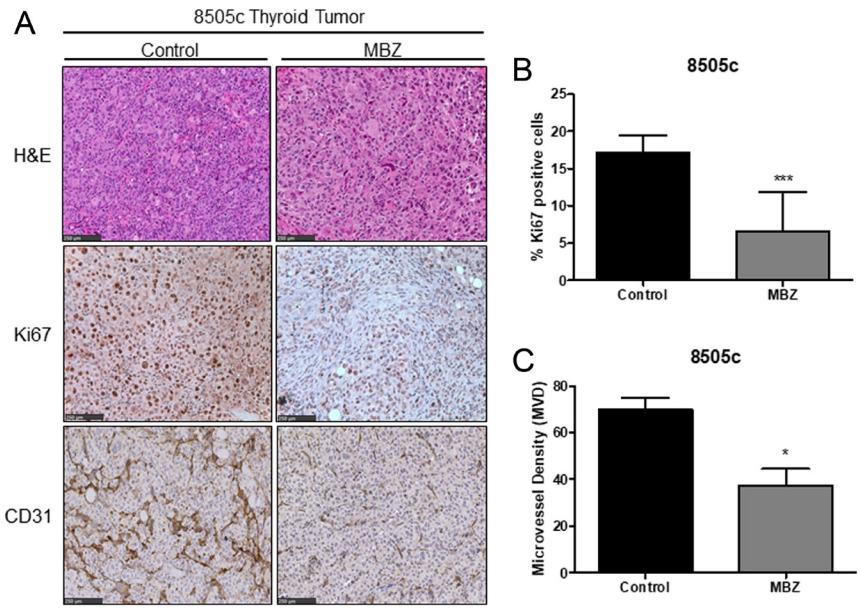

Figure 7
Mebendazole suppressed tumor cell proliferation and vascularization in orthotopic model of anaplastic thyroid cancer. (A) Immunohistochemical staining of H&E, Ki67 and CD31 in 8505c orthotopic thyroid tissue. Treatment with daily 50 mg/kg MBZ suppressed the percentage of Ki67-positive proliferating cells (B) and CD31-positive microvessel density (C) compared to untreated controls. Data represent mean ± S.D. *P* values *<0.05, ***<0.001.

a strong correlation between IC_{50} and mutation profile was not observed. B-CPAP cells were highly sensitive to MBZ-induced cell cycle arrest and apoptosis, even at low concentrations. 8505c cells exhibited a dose-dependent increase of apopstosis susceptibility to MBZ. The loss of the tumor suppressor NF2 in 8505c cells is one possible explaination for the increased resistance to apoptosis (Garcia-Rendueles *et al.* 2015). Importantly, MBZ was more effective at inducing cell death in 8505c cells than the commonly used BRAF-inhibitor, vemurafenib. Vemurafenib inhibits MAPK signaling in thyroid cancer but cells do not undergo apoptosis when treated with $BRAF^{V600E}$ inhibitors, suggesting the persistence of additional signaling pathways that promote survival and drug resistance, such as upregulated PI3K/Akt signaling (Vanden Borre *et al.* 2014).

The underlying mechanisms of MBZ that resulted in growth and metastasis suppression were further investigated in 8505c cells. We demonstrated that MBZ can suppress the migratory and invasive potential of 8505c cells in a wound healing and transwell invasion assay. This is consistent with the observed decreased expression of both p-Akt (Ser473), p-STAT3 (Y705) and Gli1 in MBZ-treated 8505c cells. This effect could be explained by upstream VEGFR2 kinase inhibition by MBZ. Although the role of abherent PI3K and Hedgehog signaling in thyroid cancer is well documented, the role of STAT3 has been more controversial. One study showed that activated STAT3 is tumor suppressive in PTC and ATC (Couto *et al.* 2012), while others have demonstrated that activated STAT3 has been shown to be significantly upregulated in PTC tumors compared to paracancerous tissue and that increased p-STAT3 corresponded with higher rates of lymph node metastasis (Zhang *et al.* 2011, Yan *et al.* 2015). The role of JAK/STAT3 signaling in promoting expansion of treatment-resistant cancer stem cells in ATC was recently demonstrated (Shiraiwa *et al.* 2019). Flubendazole, another anthelmintic benzimidazole, has been shown cause dysregulation of STAT3 activation in triple-negative breast cancer cells, resulting in decreased breast cancer cell stemness and mammosphere-forming abilities (Oh *et al.* 2018). Inhibition of STAT3 in ATC has important therapeutic implications in reducing rates of disease recurrence and increasing responsiveness to immunotherapies (Tseng *et al.* 2012, Attili *et al.* 2018). Further studies would be necessary to fully elucidate the suppressive effects of MBZ on thyroid cancer stem cell populations and its potential role in cancer immune-modulation.

In our preclinical study, we observed significant tumor growth inhibition in both B-CPAP and 8505c orthotopic thyroid models using a single, non-toxic drug. The *in vitro* difference in drug response translated into our *in vivo* studies, as treatment with MBZ caused significant regression in tumor size in the B-CPAP orthotopic tumors, whereas MBZ arrested the growth of 8505c tumors. It is worth noting that B-CPAP, although classified as a papillary carcinoma, also shares common features of poorly differentiated thyroid carcinoma (Landa *et al.* 2016). Several preclinical publications using these same models report the sensitivity of B-CPAP to a therapy but note that 8505c is largely resistant to treatment (Chan

https://erc.bioscientifica.com
https://doi.org/10.1530/ERC-19-0341

et al. 2012, Gunda *et al*. 2014, Vanden Borre *et al*. 2014). Two and three drug combinations are often needed to suppress 8505c *in vivo* (Gunda *et al*. 2014), which may translate into increased adverse drug toxicity in the clinical setting. We observed that MBZ monotherapy constrained 8505c orthotopic tumors sufficiently to prevent distant metastasis to the lung, despite the fact that widespread metastasis was seen in untreated animals. These observations have direct clinical relavance, as distant metastasis to the lungs is common in ATC patients and is a significant cause of disease-related morbidity and mortality.

The main focus of this translational study was to predict the efficacy of mebendazole in the worst thyroid cancer subtypes. These experiments indicate that mebendazole reduced cell proliferation and decreased tumor neo-vascularization *in vivo*, which is consistent with previous descriptions of the anticancer mechanism of MBZ. Smaller tumors with reduced vasculature would have less capacity to invade beyond the thyroid capsule and into surrounding lymph nodes. MBZ is known to prevent the polymerization of tubulin, the molecular target of the widely used anticancer drugs paclitaxel and vincristine, and induce mitotic arrest selectively in tumor cells without serious adverse side effects (Pinto *et al*. 2015). ATC and PDTC are aggressive, genomically heterogeneous thyroid cancers with some of the shortest predicted survivals of any cancer. In these cases, a multimodality treatment approach is likely the only way to significantly delay disease progression and increase survival. The use of a safe, non-toxic drug mebendazole as an adjuvant therapy following surgical resection or in combination with radiotherapy, targeted chemotherapy or immunotherapy could increase the durability of treatment responses in ATC, without added toxicity. Repurposed, FDA-approved drugs with known toxicity profiles, such as mebendazole, are more readily adapted to clinical trials with less risk than newly developed drugs. The evidence presented here using preclinical models of aggressive thyroid cancer subtypes, combined with the safety track record of high dose oral mebendazole, suggest a clinical trial against these cancers should be attempted.

Declaration of interest

G J R and T W are inventors on intellectual property related to mebendazole owned and managed by Johns Hopkins University conflict of interest policies. Dr Riggins is a founder of and holds equity in Benizole Therapeutics, PBC. The results of the study discussed in this publication could affect the value of Benizole. This arrangement has been reviewed and approved by the Johns Hopkins University in accordance with its conflict of interest policies. The other authors have nothing to disclose.

Funding

Funding for this study was provided by National Institutes of Health grants U01 OH10984 and U01 OH011849-01, the Virginia and D.K. Ludwig Fund, and the São Paulo Reseach Foundation (FAPESP), grant #2014/06570-6 to J M C. T B M is a recipient of a FAPESP fellowship and J M C is a recipient of a Research Productivity Scholarship of from the Brazilian National Council for Scientific and Technological Development (CNPq). G J R is supported by the Irving J. Sherman M.D. Research Professorship.

Author contribution statement

T W helped design and oversee the study, performed experiments in Figs 2, 3 and 4, assisted in mouse studies and histology in Figs 5, 6 and 7 and drafted the paper, T B M performed experiment in Fig. 1, conducted mouse studies and histology in Figs 5, 6 and 7 and helped write the paper, N J performed drug treatment and western blot experiments in Figs 3 and 4, J M C and G J R jointly help design the experiments, reviewed the data, and edited the paper.

References

Alonso-Gordoa T, Diez JJ, Duran M & Grande E 2015 Advances in thyroid cancer treatment: latest evidence and clinical potential. *Therapeutic Advances in Medical Oncology* **7** 22–38. (https://doi.org/10.1177/1758834014551936)

Antonello ZA & Nucera C 2014 Orthotopic mouse models for the preclinical and translational study of targeted therapies against metastatic human thyroid carcinoma with BRAF(V600E) or wild-type BRAF. *Oncogene* **33** 5397–5404. (https://doi.org/10.1038/onc.2013.544)

Attili I, Karachaliou N, Bonanno L, Berenguer J, Bracht J, Codony-Servat J, Codony-Servat C, Ito M & Rosell R 2018 STAT3 as a potential immunotherapy biomarker in oncogene-addicted non-small cell lung cancer. *Therapeutic Advances in Medical Oncology* **10** 1758835918763744. (https://doi.org/10.1177/1758835918763744)

Bai RY, Staedtke V, Aprhys CM, Gallia GL & Riggins GJ 2011 Antiparasitic mebendazole shows survival benefit in 2 preclinical models of glioblastoma multiforme. *Neuro-Oncology* **13** 974–982. (https://doi.org/10.1093/neuonc/nor077)

Bai RY, Staedtke V, Rudin CM, Bunz F & Riggins GJ 2015 Effective treatment of diverse medulloblastoma models with mebendazole and its impact on tumor angiogenesis. *Neuro-Oncology* **17** 545–554. (https://doi.org/10.1093/neuonc/nou234)

Bates MF, Lamas MR, Randle RW, Long KL, Pitt SC, Schneider DF & Sippel RS 2018 Back so soon? Is early recurrence of papillary thyroid cancer really just persistent disease? *Surgery* **163** 118–123. (https://doi.org/10.1016/j.surg.2017.05.028)

Cancer Genome Atlas Research Network 2014 Integrated genomic characterization of papillary thyroid carcinoma. *Cell* **159** 676–690. (https://doi.org/10.1016/j.cell.2014.09.050)

Chan CM, Jing X, Pike LA, Zhou Q, Lim DJ, Sams SB, Lund GS, Sharma V, Haugen BR & Schweppe RE 2012 Targeted inhibition of Src kinase with dasatinib blocks thyroid cancer growth and metastasis. *Clinical Cancer Research* **18** 3580–3591. (https://doi.org/10.1158/1078-0432.CCR-11-3359)

Cohen EE, Rosen LS, Vokes EE, Kies MS, Forastiere AA, Worden FP, Kane MA, Sherman E, Kim S, Bycott P, *et al*. 2008 Axitinib is an active treatment for all histologic subtypes of advanced thyroid cancer: results from a phase II study. *Journal of Clinical Oncology* **26** 4708–4713. (https://doi.org/10.1200/JCO.2007.15.9566)

Couto JP, Daly L, Almeida A, Knauf JA, Fagin JA, Sobrinho-Simoes M, Lima J, Maximo V, Soares P, Lyden D, *et al*. 2012 STAT3 negatively

https://erc.bioscientifica.com
https://doi.org/10.1530/ERC-19-0341

regulates thyroid tumorigenesis. *PNAS* **109** E2361–E2370. (https://doi.org/10.1073/pnas.1201232109)

Czarniecka A, Oczko-Wojciechowska M & Barczynski M 2016 BRAF V600E mutation in prognostication of papillary thyroid cancer (PTC) recurrence. *Gland Surgery* **5** 495–505. (https://doi.org/10.21037/gs.2016.09.09)

De Crevoisier R, Baudin E, Bachelot A, Leboulleux S, Travagli JP, Caillou B & Schlumberger M 2004 Combined treatment of anaplastic thyroid carcinoma with surgery, chemotherapy, and hyperfractionated accelerated external radiotherapy. *International Journal of Radiation Oncology, Biology, Physics* **60** 1137–1143. (https://doi.org/10.1016/j.ijrobp.2004.05.032)

Dobrosotskaya IY, Hammer GD, Schteingart DE, Maturen KE & Worden FP 2011 Mebendazole monotherapy and long-term disease control in metastatic adrenocortical carcinoma. *Endocrine Practice* **17** e59–e62. (https://doi.org/10.4158/EP10390.CR)

Doudican N, Rodriguez A, Osman I & Orlow SJ 2008 Mebendazole induces apoptosis via Bcl-2 inactivation in chemoresistant melanoma cells. *Molecular Cancer Research* **6** 1308–1315. (https://doi.org/10.1158/1541-7786.MCR-07-2159)

Doudican NA, Byron SA, Pollock PM & Orlow SJ 2013 XIAP downregulation accompanies mebendazole growth inhibition in melanoma xenografts. *Anti-Cancer Drugs* **24** 181–188. (https://doi.org/10.1097/CAD.0b013e32835a43f1)

Elisei R, Ugolini C, Viola D, Lupi C, Biagini A, Giannini R, Romei C, Miccoli P, Pinchera A & Basolo F 2008 BRAF(V600E) mutation and outcome of patients with papillary thyroid carcinoma: a 15-year median follow-up study. *Journal of Clinical Endocrinology and Metabolism* **93** 3943–3949. (https://doi.org/10.1210/jc.2008-0607)

Garcia-Rendueles ME, Ricarte-Filho JC, Untch BR, Landa I, Knauf JA, Voza F, Smith VE, Ganly I, Taylor BS, Persaud Y, *et al*. 2015 NF2 loss promotes oncogenic RAS-induced thyroid cancers via YAP-dependent transactivation of RAS proteins and sensitizes them to MEK inhibition. *Cancer Discovery* **5** 1178–1193. (https://doi.org/10.1158/2159-8290.CD-15-0330)

Guerra A, Di Crescenzo V, Garzi A, Cinelli M, Carlomagno C, Tonacchera M, Zeppa P & Vitale M 2013 Genetic mutations in the treatment of anaplastic thyroid cancer: a systematic review. *BMC Surgery* **13** (Supplement 2) S44. (https://doi.org/10.1186/1471-2482-13-S2-S44)

Gunda V, Bucur O, Varnau J, Vanden Borre P, Bernasconi MJ, Khosravi-Far R & Parangi S 2014 Blocks to thyroid cancer cell apoptosis can be overcome by inhibition of the MAPK and PI3K/AKT pathways. *Cell Death and Disease* **5** e1104. (https://doi.org/10.1038/cddis.2014.78)

Haddad RI, Lydiatt WM, Ball DW, Busaidy NL, Byrd D, Callender G, Dickson P, Duh QY, Ehya H, Haymart M, *et al*. 2015 Anaplastic thyroid carcinoma, Version 2.2015. *Journal of the National Comprehensive Cancer Network* **13** 1140–1150.

Hsu KT, Yu XM, Audhya AW, Jaume JC, Lloyd RV, Miyamoto S, Prolla TA & Chen H 2014 Novel approaches in anaplastic thyroid cancer therapy. *Oncologist* **19** 1148–1155. (https://doi.org/10.1634/theoncologist.2014-0182)

Jo YS, Li S, Song JH, Kwon KH, Lee JC, Rha SY, Lee HJ, Sul JY, Kweon GR, Ro HK, *et al*. 2006 Influence of the BRAF V600E mutation on expression of vascular endothelial growth factor in papillary thyroid cancer. *Journal of Clinical Endocrinology and Metabolism* **91** 3667–3670. (https://doi.org/10.1210/jc.2005-2836)

Keefe SM, Cohen MA & Brose MS 2010 Targeting vascular endothelial growth factor receptor in thyroid cancer: the intracellular and extracellular implications. *Clinical Cancer Research* **16** 778–783. (https://doi.org/10.1158/1078-0432.CCR-08-2743)

Keutgen XM, Sadowski SM & Kebebew E 2015 Management of anaplastic thyroid cancer. *Gland Surgery* **4** 44–51. (https://doi.org/10.3978/j.issn.2227-684X.2014.12.02)

Kim S, Park YW, Schiff BA, Doan DD, Yazici Y, Jasser SA, Younes M, Mandal M, Bekele BN & Myers JN 2005 An orthotopic model of anaplastic thyroid carcinoma in athymic nude mice. *Clinical Cancer Research* **11** 1713–1721. (https://doi.org/10.1158/1078-0432.CCR-04-1908)

Kurebayashi J, Otsuki T, Tanaka K, Yamamoto Y, Moriya T & Sonoo H 2003 Medroxyprogesterone acetate decreases secretion of interleukin-6 and parathyroid hormone-related protein in a new anaplastic thyroid cancer cell line, KTC-2. *Thyroid* **13** 249–258.

Landa I, Ganly I, Chan TA, Mitsutake N, Matsuse M, Ibrahimpasic T, Ghossein RA & Fagin JA 2013 Frequent somatic tert promoter mutations in thyroid cancer: higher prevalence in advanced forms of the disease. *Journal of Clinical Endocrinology and Metabolism* **98** E1562–E1566. (https://doi.org/10.1210/jc.2013-2383)

Landa I, Ibrahimpasic T, Boucai L, Sinha R, Knauf JA, Shah RH, Dogan S, Ricarte-Filho JC, Krishnamoorthy GP, Xu B, *et al*. 2016 Genomic and transcriptomic hallmarks of poorly differentiated and anaplastic thyroid cancers. *Journal of Clinical Investigation* **126** 1052–1066. (https://doi.org/10.1172/JCI85271)

Larsen AR, Bai RY, Chung JH, Borodovsky A, Rudin CM, Riggins GJ & Bunz F 2015 Repurposing the antihelmintic mebendazole as a hedgehog inhibitor. *Molecular Cancer Therapeutics* **14** 3–13. (https://doi.org/10.1158/1535-7163.MCT-14-0755-T)

Lim H, Devesa SS, Sosa JA, Check D & Kitahara CM 2017 Trends in thyroid cancer incidence and mortality in the United States, 1974–2013. *JAMA* **317** 1338–1348. (https://doi.org/10.1001/jama.2017.2719)

Liu R & Xing M 2016 Tert promoter mutations in thyroid cancer. *Endocrine-Related Cancer* **23** R143–R155. (https://doi.org/10.1530/ERC-15-0533)

Liu X, Bishop J, Shan Y, Pai S, Liu D, Murugan AK, Sun H, El-Naggar AK & Xing M 2013 Highly prevalent tert promoter mutations in aggressive thyroid cancers. *Endocrine-Related Cancer* **20** 603–610. (https://doi.org/10.1530/ERC-13-0210)

Melck AL, Yip L & Carty SE 2010 The utility of BRAF testing in the management of papillary thyroid cancer. *Oncologist* **15** 1285–1293. (https://doi.org/10.1634/theoncologist.2010-0156)

Morrison JA, Pike LA, Lund G, Zhou Q, Kessler BE, Bauerle KT, Sams SB, Haugen BR & Schweppe RE 2015 Characterization of thyroid cancer cell lines in murine orthotopic and intracardiac metastasis models. *Hormones and Cancer* **6** 87–99. (https://doi.org/10.1007/s12672-015-0219-0)

Mudduluru G, Walther W, Kobelt D, Dahlmann M, Treese C, Assaraf YG & Stein U 2016 Repositioning of drugs for intervention in tumor progression and metastasis: old drugs for new targets. *Drug Resistance Updates* **26** 10–27. (https://doi.org/10.1016/j.drup.2016.03.002)

Mukhopadhyay T, Sasaki J, Ramesh R & Roth JA 2002 Mebendazole elicits a potent antitumor effect on human cancer cell lines both in vitro and in vivo. *Clinical Cancer Research* **8** 2963–2969.

Nagaiah G, Hossain A, Mooney CJ, Parmentier J & Remick SC 2011 Anaplastic thyroid cancer: a review of epidemiology, pathogenesis, and treatment. *Journal of Oncology* **2011** 542358. (https://doi.org/10.1155/2011/542358)

Nucera C, Nehs MA, Mekel M, Zhang X, Hodin R, Lawler J, Nose V & Parangi S 2009 A novel orthotopic mouse model of human anaplastic thyroid carcinoma. *Thyroid* **19** 1077–1084. (https://doi.org/10.1089/thy.2009.0055)

Nygren P & Larsson R 2014 Drug repositioning from bench to bedside: tumour remission by the antihelmintic drug mebendazole in refractory metastatic colon cancer. *Acta Oncologica* **53** 427–428. (https://doi.org/10.3109/0284186X.2013.844359)

Nygren P, Fryknas M, Agerup B & Larsson R 2013 Repositioning of the anthelmintic drug mebendazole for the treatment for colon cancer. *Journal of Cancer Research and Clinical Oncology* **139** 2133–2140. (https://doi.org/10.1007/s00432-013-1539-5)

Oh E, Kim YJ, An H, Sung D, Cho TM, Farrand L, Jang S, Seo JH & Kim JY 2018 Flubendazole elicits anti-metastatic effects in triple-negative breast cancer via STAT3 inhibition. *International Journal of Cancer* **143** 1978–1993. (https://doi.org/10.1002/ijc.31585)

O'Neill JP & Shaha AR 2013 Anaplastic thyroid cancer. *Oral Oncology* **49** 702–706. (https://doi.org/10.1016/j.oraloncology.2013.03.440)

Pantziarka P, Bouche G, Meheus L, Sukhatme V & Sukhatme VP 2014 Repurposing drugs in oncology (ReDO)-mebendazole as an anti-cancer agent. *Ecancermedicalscience* **8** 443. (https://doi.org/10.3332/ecancer.2014.443)

Perri F, Lorenzo GD, Scarpati GD & Buonerba C 2011 Anaplastic thyroid carcinoma: a comprehensive review of current and future therapeutic options. *World Journal of Clinical Oncology* **2** 150–157. (https://doi.org/10.5306/wjco.v2.i3.150)

Pinto LC, Soares BM, Pinheiro Jde J, Riggins GJ, Assumpcao PP, Burbano RM & Montenegro RC 2015 The anthelmintic drug mebendazole inhibits growth, migration and invasion in gastric cancer cell model. *Toxicology In Vitro* **29** 2038–2044. (https://doi.org/10.1016/j.tiv.2015.08.007)

Ragazzi M, Ciarrocchi A, Sancisi V, Gandolfi G, Bisagni A & Piana S 2014 Update on anaplastic thyroid carcinoma: morphological, molecular, and genetic features of the most aggressive thyroid cancer. *International Journal of Endocrinology* **2014** 790834. (https://doi.org/10.1155/2014/790834)

Saini S, Tulla K, Maker AV, Burman KD & Prabhakar BS 2018 Therapeutic advances in anaplastic thyroid cancer: a current perspective. *Molecular Cancer* **17** 154. (https://doi.org/10.1186/s12943-018-0903-0)

Saiselet M, Floor S, Tarabichi M, Dom G, Hebrant A, van Staveren WC & Maenhaut C 2012 Thyroid cancer cell lines: an overview. *Frontiers in Endocrinology* **3** 133. (https://doi.org/10.3389/fendo.2012.00133)

Sasaki J, Ramesh R, Chada S, Gomyo Y, Roth JA & Mukhopadhyay T 2002 The anthelmintic drug mebendazole induces mitotic arrest and apoptosis by depolymerizing tubulin in non-small cell lung cancer cells. *Molecular Cancer Therapeutics* **1** 1201–1209.

Schweppe RE 2012 Thyroid cancer cell lines: critical models to study thyroid cancer biology and new therapeutic targets. *Frontiers in Endocrinology* **3** 81. (https://doi.org/10.3389/fendo.2012.00081)

Sherman SI 2011 Targeted therapies for thyroid tumors. *Modern Pathology* **24** (Supplement 2) S44–S52. (https://doi.org/10.1038/modpathol.2010.165)

Sherman SI, Wirth LJ, Droz JP, Hofmann M, Bastholt L, Martins RG, Licitra L, Eschenberg MJ, Sun YN, Juan T, *et al*. 2008 Motesanib diphosphate in progressive differentiated thyroid cancer. *New England Journal of Medicine* **359** 31–42. (https://doi.org/10.1056/NEJMoa075853)

Shiraiwa K, Matsuse M, Nakazawa Y, Ogi T, Suzuki K, Saenko V, Xu S, Umezawa K, Yamashita S, Tsukamoto K, *et al*. 2019 JAK/STAT3 and NF-kappaB signaling pathways regulate cancer stem-cell properties in anaplastic thyroid cancer cells. *Thyroid* **29** 674–682. (https://doi.org/10.1089/thy.2018.0212)

Simbulan-Rosenthal CM, Dakshanamurthy S, Gaur A, Chen YS, Fang HB, Abdussamad M, Zhou H, Zapas J, Calvert V, Petricoin EF, *et al*. 2017 The repurposed anthelmintic mebendazole in combination with trametinib suppresses refractory NRASQ61K melanoma. *Oncotarget* **8** 12576–12595. (https://doi.org/10.18632/oncotarget.14990)

Skibinski CG, Williamson T & Riggins GJ 2018 Mebendazole and radiation in combination increase survival through anticancer mechanisms in an intracranial rodent model of malignant meningioma. *Journal of Neuro-Oncology* **140** 529–538. (https://doi.org/10.1007/s11060-018-03009-7)

Song YS & Park YJ 2019 Genomic characterization of differentiated thyroid carcinoma. *Endocrinology and Metabolism* **34** 1–10. (https://doi.org/10.3803/EnM.2019.34.1.1)

Tan Z, Chen L & Zhang S 2016 Comprehensive modeling and discovery of mebendazole as a novel TRAF2- and NCK-interacting kinase inhibitor. *Scientific Reports* **6** 33534. (https://doi.org/10.1038/srep33534)

Tseng LM, Huang PI, Chen YR, Chen YC, Chou YC, Chen YW, Chang YL, Hsu HS, Lan YT, Chen KH, *et al*. 2012 Targeting signal transducer and activator of transcription 3 pathway by cucurbitacin I diminishes self-renewing and radiochemoresistant abilities in thyroid cancer-derived CD133+ cells. *Journal of Pharmacology and Experimental Therapeutics* **341** 410–423. (https://doi.org/10.1124/jpet.111.188730)

Vanden Borre P, Gunda V, McFadden DG, Sadow PM, Varmeh S, Bernasconi M & Parangi S 2014 Combined BRAF(V600E)- and SRC-inhibition induces apoptosis, evokes an immune response and reduces tumor growth in an immunocompetent orthotopic mouse model of anaplastic thyroid cancer. *Oncotarget* **5** 3996–4010. (https://doi.org/10.18632/oncotarget.2130)

Vicari L, Colarossi C, Giuffrida D, De Maria R & Memeo L 2016 Cancer stem cells as a potential therapeutic target in thyroid carcinoma. *Oncology Letters* **12** 2254–2260. (https://doi.org/10.3892/ol.2016.4936)

Viglietto G, Maglione D, Rambaldi M, Cerutti J, Romano A, Trapasso F, Fedele M, Ippolito P, Chiappetta G & Botti G 1995 Upregulation of vascular endothelial growth factor (VEGF) and downregulation of placenta growth factor (PlGF) associated with malignancy in human thyroid tumors and cell lines. *Oncogene* **11** 1569–1579.

Viola D, Valerio L, Molinaro E, Agate L, Bottici V, Biagini A, Lorusso L, Cappagli V, Pieruzzi L, Giani C, *et al*. 2016 Treatment of advanced thyroid cancer with targeted therapies: ten years of experience. *Endocrine-Related Cancer* **23** R185–R205. (https://doi.org/10.1530/ERC-15-0555)

Williamson AJ, Doscas ME, Ye J, Heiden KB, Xing M, Li Y, Prinz RA & Xu X 2016*a* The sonic hedgehog signaling pathway stimulates anaplastic thyroid cancer cell motility and invasiveness by activating Akt and c-Met. *Oncotarget* **7** 10472–10485. (https://doi.org/10.18632/oncotarget.7228)

Williamson T, Bai RY, Staedtke V, Huso D & Riggins GJ 2016*b* Mebendazole and a non-steroidal anti-inflammatory combine to reduce tumor initiation in a colon cancer preclinical model. *Oncotarget* **7** 68571–68584. (https://doi.org/10.18632/oncotarget.11851)

Xing M 2013 Molecular pathogenesis and mechanisms of thyroid cancer. *Nature Reviews: Cancer* **13** 184–199. (https://doi.org/10.1038/nrc3431)

Yan LI, Li LI, Li Q, Di W, Shen W, Zhang L & Guo H 2015 Expression of signal transducer and activator of transcription 3 and its phosphorylated form is significantly upregulated in patients with papillary thyroid cancer. *Experimental and Therapeutic Medicine* **9** 2195–2201. (https://doi.org/10.3892/etm.2015.2409)

Yoo SK, Song YS, Lee EK, Hwang J, Kim HH, Jung G, Kim YA, Kim SJ, Cho SW, Won JK, *et al*. 2019 Integrative analysis of genomic and transcriptomic characteristics associated with progression of aggressive thyroid cancer. *Nature Communications* **10** 2764. (https://doi.org/10.1038/s41467-019-10680-5)

Yun JY, Kim YA, Choe JY, Min H, Lee KS, Jung Y, Oh S & Kim JE 2014 Expression of cancer stem cell markers is more frequent in anaplastic thyroid carcinoma compared to papillary thyroid carcinoma and is related to adverse clinical outcome. *Journal of Clinical Pathology* **67** 125–133. (https://doi.org/10.1136/jclinpath-2013-201711)

Zhang J, Gill A, Atmore B, Johns A, Delbridge L, Lai R & McMullen T 2011 Upregulation of the signal transducers and activators of transcription 3 (STAT3) pathway in lymphatic metastases of papillary thyroid cancer. *International Journal of Clinical and Experimental Pathology* **4** 356–362.

Received in final form 9 December 2019
Accepted 16 December 2019
Accepted Manuscript published online 17 December 2019